Automatic Approach to Detect Ice Sheet Margin Using ERS-1 Synthetic Aperture Radar Imagery

Hong-Gyoo Sohn* and Kenneth C. Jezek
Byrd Polar Research Center and
*Department of Civil and Environmental Engineering and Geodetic Science
The Ohio State University
Columbus, OH 43210, USA

Commission VII, Working Group 8

KEY WORDS: SAR, SPOT, Aerial Photography, Change_Detection

ABSTRACT

A portion of the Greenland ice sheet margin near the Jakobshavn glacier is mapped using an automatic approach applied to ERS-1 Synthetic Aperture Radar (SAR) imagery, visible imagery (SPOT), and a digitized aerial photograph. This process involves integration of an anisotropic diffusion algorithm, a local dynamic thresholding method, and a recursive edge following scheme.

1. INTRODUCTION

Polar ice sheet margins are sensitive indicators of changing climate. For example, melting at the margin of the ice sheet in Greenland will increase by 0.5 m water/a for each degree increase in summer temperature (Braithwaite and Olsesen, 1993). Based on repeated mapping of glacier systems in West Greenland, glacier margin advances and recessions of the ice sheet margin parallel prevailing climatic trends (Weidick et al., 1992). This suggests that consistent and long-term observations of the ice sheet margin change may provide a useful indicator of changing climate.

An ice sheet margin detection algorithm is implemented to monitor and detect ice sheet margin fluctuations using visible and microwave imagery. A portion of the Greenland ice sheet margin near the Jakobshavn glacier (Fig. 1) is mapped using an automatic approach applied to ERS-1 SAR imagery, visible imagery (SPOT), and a digitized aerial photograph.

2. STUDY AREA AND DATA SETS

The aerial photograph was taken on July 10, 1985. The SPOT panchromatic image and the ERS-1 SAR image were obtained May 30, 1988 and August 20, 1992, respectively. The coverage area of the SAR image is about 100 x 100 km. The coverage area of SPOT and the aerial photograph is about 60 x 60 km and 37.5 x 37.5 km, respectively.

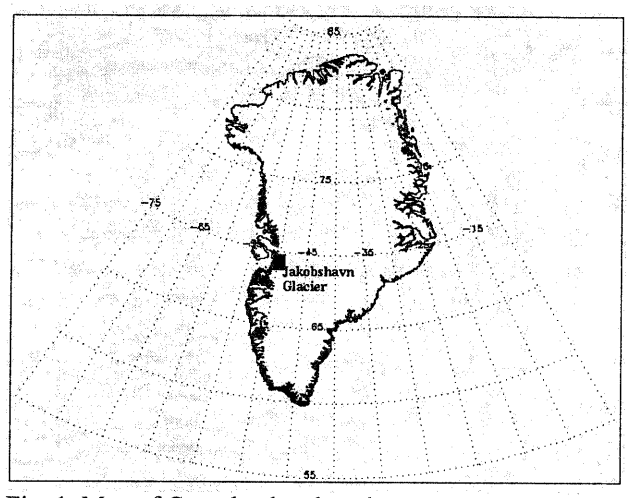

Fig. 1. Map of Greenland and study area

3. APPROACH

Image tone and texture variations are used to map the ice sheet margin. Fig. 2 schematically depicts the approach for detecting ice sheet margin using the imagery.

The ice sheet margin is detected by sequential application of several different algorithms. First, the original ERS-1 SAR imagery is geocoded and terrain corrected using the available digital elevation model produced in Denmark at Kort- og Matrikelstyrelsen (KMS) (Tscherning et al., 1992) (Fig. 3). The SPOT imagery and the digitized aerial photograph are also geocoded using ground control points from 1:50,000 scale orthophotos (Brecher, personal communication) (Fig. 4, 5). All imagery are resampled to 50 m resolution. After geocoding, the overlapping area is used for all subsequent algorithmic processing.

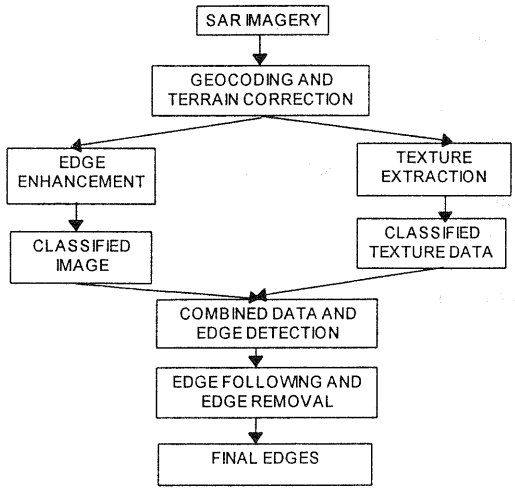

Fig. 2. Schematic diagram for ice sheet margin detection using ERS-1 SAR imagery.

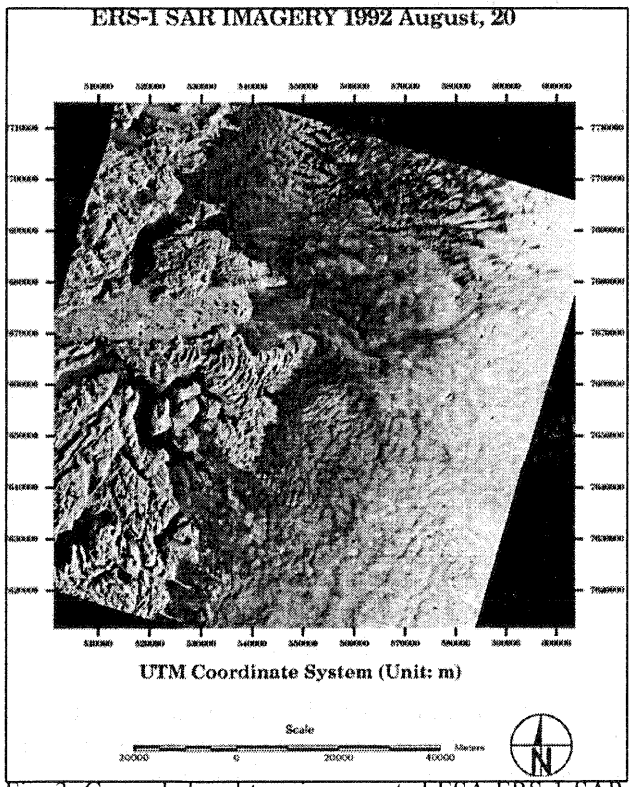

Fig. 3. Geocoded and terrain corrected ESA ERS-1 SAR imagery of August 20, 1992 with 50 m resolution.

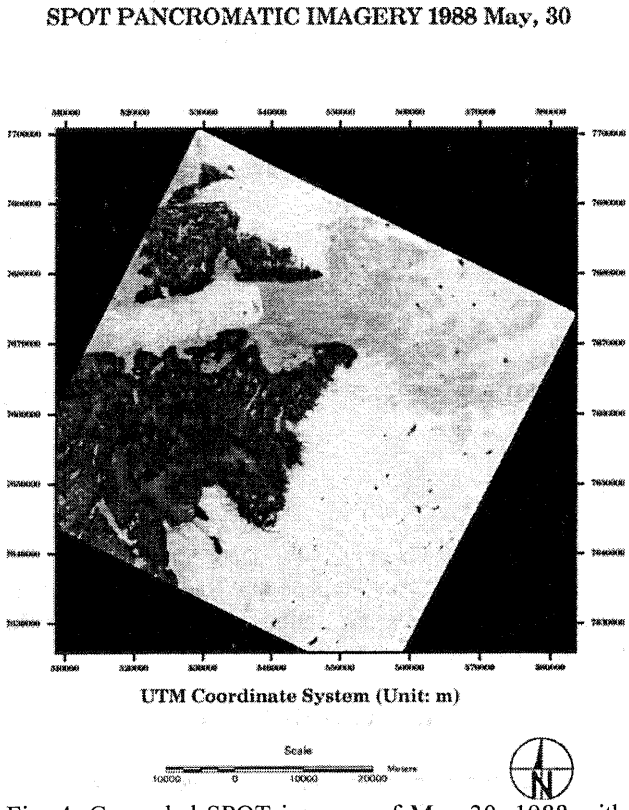

Fig. 4. Geocoded SPOT imagery of May 30, 1988 with 50 m resolution.

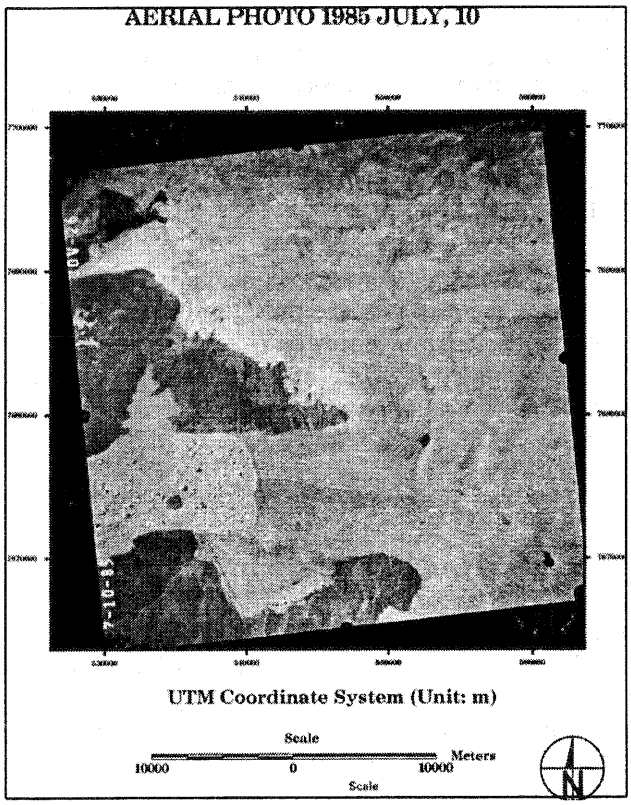

Fig. 5. Geocoded digitized aerial photograph of July 10, 1985 with 50 m resolution.

Next, an anisotropic diffusion algorithm (Perona and Makik, 1990) is used on the SAR image to minimize noise while preserving the position and magnitude of the edges. Anisotropic diffusion applies a four pixel operator to each pixel in a digital image. The equation for computing a new pixel value in the sequence is

$$I_{i,j}^{t+1} = I_{i,j}^{t} + \lambda(C_N \cdot \nabla_N I + C_S \cdot \nabla_S I + C_E \cdot \nabla_E I + C_W \cdot \nabla_W I) \quad (1)$$

where

$I_{i,j}^{t+1}$ the new central pixel ($(t+1)$th iterations) in ith row, jth column

$I_{i,j}^{t}$ the current central pixel (tth iterations) in ith row , jth column

λ a weight value (0.25 is used)

c_N, c_S, c_E, c_W directional diffusion coefficients (a function of ∇I) , (N:north, S:south, W:west, E:east)

∇I a gradient (4 neighboring pixel - central pixel).

The functional form used for the directional diffusion coefficients C_N, C_S, C_E, C_W is,

$$C(\nabla I) = \left(1 + \left(\frac{\|\nabla I\|}{K} \right)^2 \right)^{-1} \quad (2)$$

where K = the gradient threshold.

Fig. 6 shows the resultant image after applying the anisotropic diffusion algorithm to Fig. 3 for K=5 and iterations=50.

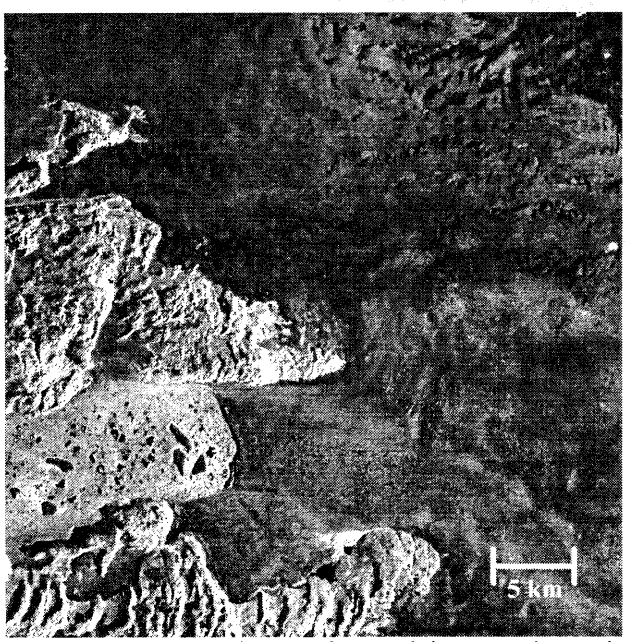

Fig. 6. The resultant image after applying an anisotropic diffusion algorithm on Fig. 3 (K=5, iterations=50).

Texture data are created using second order statistics in a small-area image patch selected on the SAR image. A local dynamic thresholding algorithm (Haverkamp et al., 1995) was applied to both the edge enhanced image (Fig. 6) and the resultant texture data. This algorithm segments the image into three different gray level classes.

Fig. 7 is the classified image obtained after applying the local dynamic thresholding algorithm to Fig. 6. Fig. 8 is the classified image obtained from the texture data.

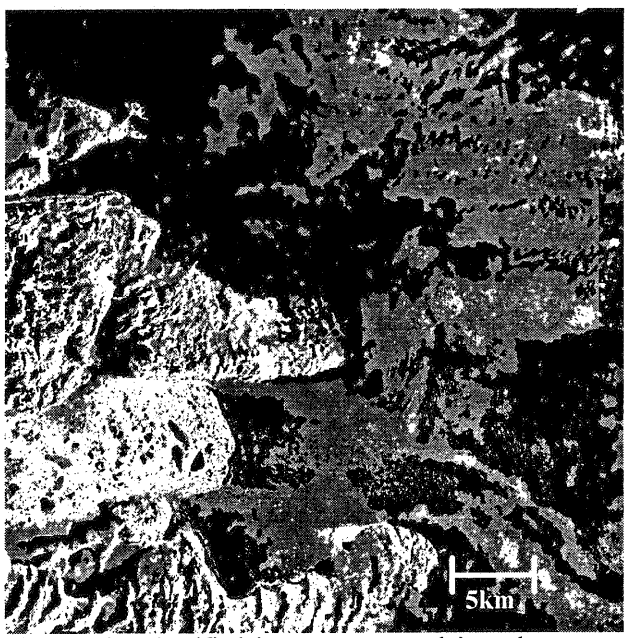

Fig. 7. The classified image segmented into three gray level classes after applying dynamic thresholding algorithm to Fig. 6 .

Fig. 8. The classified image segmented into three gray level classes after applying the dynamic thresholding method to gray level converted texture data.

A final image was created by combining the classified images of Fig. 7 and Fig. 8. This was done by selecting the same gray level class, for example the rock, in both Fig. 7 and Fig. 8, and then filtering out the other two classes. Edge detection was performed on the final image using the Roberts edge detection algorithm (Pratt, 1978). Fig. 9 is the image of detected edges.

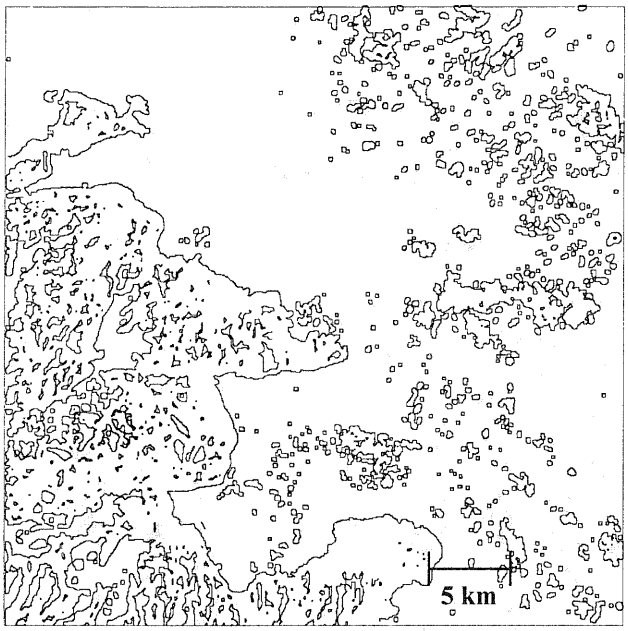

Fig. 9. Detected edges after applying Roberts edge detection algorithm to the final image.

A recursive line following scheme is implemented by using a chain code (Ballard and Brown, 1982) to detect the short, unwanted edges. The binary line image is scanned line by line for points from which to start a chain. Every continuous line is chain coded and the length for each line is stored. A global constraint on length is set to identify the ice sheet boundary and remove the unwanted small edges.

The detection of ice sheet boundaries using SPOT imagery and the digitized aerial photograph was done using image tone information. First, an anisotropic diffusion method was applied to both images to enhance edges. A dynamic thresholding algorithm was then applied to both edge enhanced images. Fig. 10 and Fig. 11 are classified images segmented into three gray level classes after application of the dynamic thresholding algorithm to the edge enhanced SPOT image and the digitized aerial photograph, respectively. The final images were created by selecting the class(es) corresponding to the rock area and filtering out the other class(es) from both Fig. 10 and Fig. 11. Edge detection is performed on the final images using the Roberts edge detection algorithm. Recursive edge following is done to detect the boundaries.

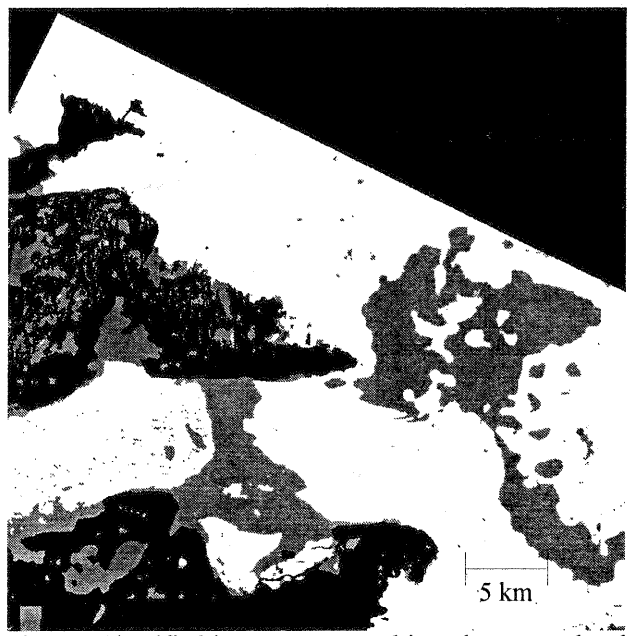

Fig. 10. Classified image segmented into three gray level classes after applying dynamic thresholding algorithm to the edge enhanced SPOT image.

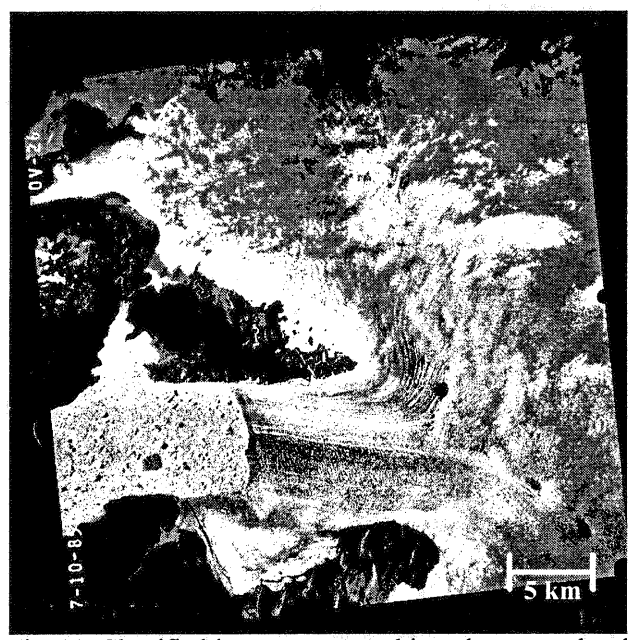

Fig. 11. Classified image segmented into three gray level classes after applying the dynamic thresholding algorithm to the edge enhanced aerial photograph.

4. RESULTS

Fig. 12 is the final result of the detected ice sheet boundary from ERS-1 SAR imagery. The constraint used for the length of edge was 1900 pixels (size of image is 750 x 750 pixels).

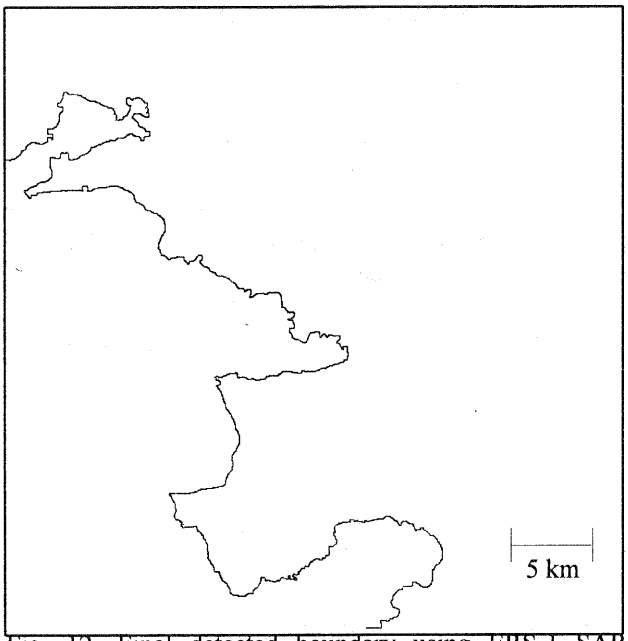

Fig. 12. Final detected boundary using ERS-1 SAR imagery after removing unwanted edges.

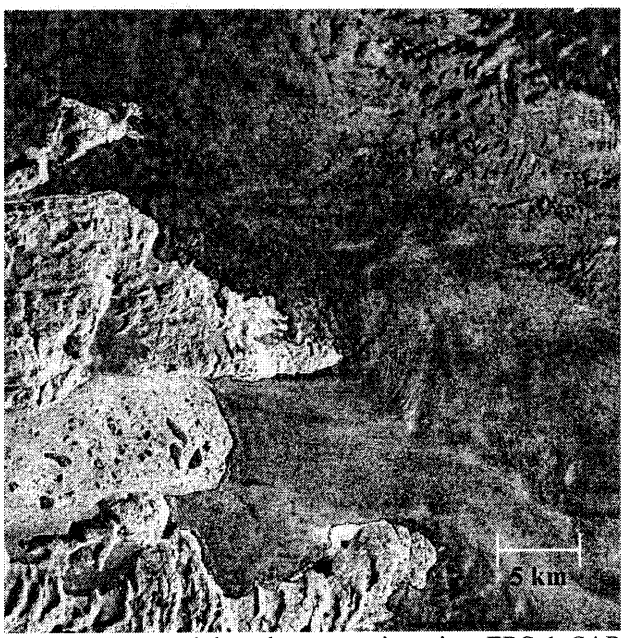

Fig. 13. Detected ice sheet margin using ERS-1 SAR imagery (Fig. 10) draped over Fig. 3.

Fig. 13 shows the detected ice sheet boundary draped on Fig. 3. Fig. 14 and Fig. 15 represent detected ice sheet boundaries for the SPOT and the digitized aerial photograph draped over Fig. 4 and Fig. 5, respectively. The detected ice sheet boundary matches the visually-inspected ice sheet margin to within several pixels (150 m).

The three ice sheet boundaries produced from ERS-1 SAR imagery, SPOT, and the digitized aerial photograph are compared (Fig. 16). The upper and lower parts of Fig. 16 show that the ice sheet margin detected using the SAR imagery is several hundred meters outside of the ice sheet margin detected using the visible imagery. This is mainly caused by the uncertainty in the digital elevation model used to terrain correct the SAR imagery.

In the middle part of Fig. 16, the ice sheet margin detected using the SAR imagery shows more variation than the visible imagery. This seems to be mainly due to different image signatures near the ice sheet margin. The SAR penetrates the surface snow and may include signals from the surface, volume and underlying rock. The visible imagery only maps the surface features.

The ice sheet margins detected using different data sets show that over a 7 year period (1985-1992) the ice sheet margin north and south of the Jakobshavn glacier fluctuates by less than 350 m. The calving front fluctuates up to 2.8 km.

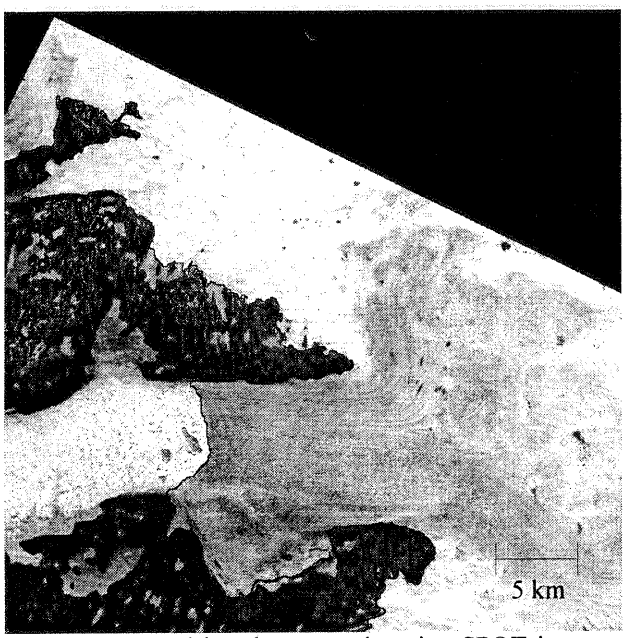

Fig. 14. Detected ice sheet margin using SPOT imagery draped over Fig. 4.

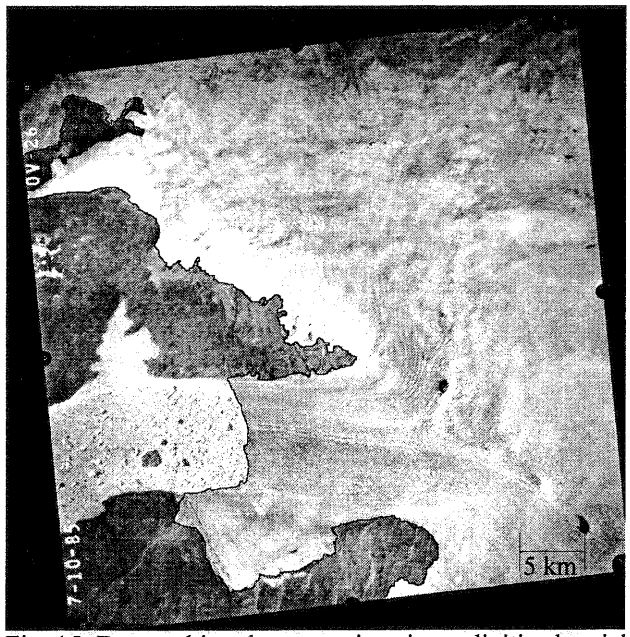

Fig. 15. Detected ice sheet margin using a digitized aerial photograph draped over Fig. 5.

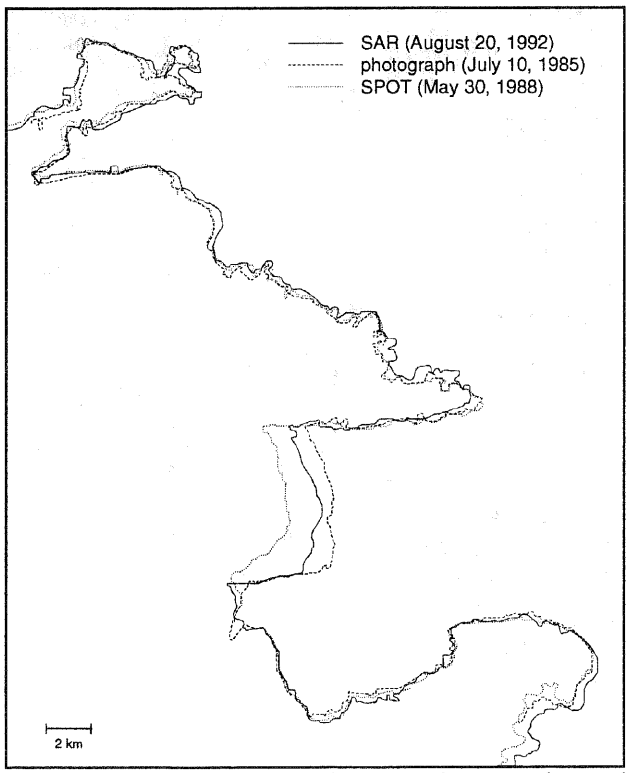

Fig. 16. Comparison of ice sheet margin maps detected using three different sensors.

5. CONCLUSIONS

Steps for ice sheet margin extraction were presented by integrating several different algorithms and applying them to different sensor data sets. By comparing the ice sheet margin detected using different data, the following conclusions are reached.

- The ice sheet margin is successfully detected using an automatic approach.
- Each sensor (SAR, SPOT, aerial photograph) has a different image signature near the ice sheet margin which causes an apparent fluctuation in the ice sheet margin.
- Uncertainty of digital elevation model causes displacement of the margin up to several hundred meters in geocoded and terrain corrected SAR imagery.
- Over a 7 year period the ice sheet margin north and south of the Jakobshavn glacier fluctuates by less than 350 m. The calving front fluctuates up to 2.8 km.

6. REFERENCES

Ballad, DH and Brown, CM, 1982, Computer Vision, Prentice-Hall, Inc., New Jersey.

Braihwaite, R.J., Olsesen, O.B., 1993, Seasonal variation of ice ablation at the margin of the Greenland ice sheet and its sensitivity to climate change, Qamanarssup sermia, West Greenland, Journal of Glaciology, Vol. 39, No. 132, pp. 267-274.

Haverkamp, D., Soh, L.K., and Tsatsoulis, C., 1995, A Comprehensive, Automated Approach to Determining Sea Ice Thickness from SAR Data, IEEE Transactions On Geoscience and Remote Sensing, Vol. 33, No. 1, pp. 46-57.

Perona, P. and Malik, J., 1990, Scale-Space and Edge Detection Using Anisotropic Diffusion, IEEE Transactions on PAMI, Vol. 12, No. 7, pp. 629-639.

Pratt, W.K., 1978, Digital Image Processing, John Wiley & Sons, Inc.

Tscherning, C.C., Knudsen, P., Ekholm, S., and Andersen, O.B., 1992, An Analysis of The Gravity Field In The Norwegian Sea And Mapping of The Ice Cap of Greenland Using ERS-1 Altimeter Measurements, Proceedings First ERS-1 Symposium, Cannes, France, 4-6 November.

Weidick, A., Boggild, C.E., and Knudsen, N.T., 1992, Glacier inventory and atlas of West Greenland, Grønlands Geologiske Undersøgelse, Rapport 158.